EVS30 Symposium
Stuttgart, Germany, October 9 - 11, 2017

Wireless Power Transfer for Railway Vehicles

Nejila Parspour[1], Philipp Seitz[1], Anna Lusiewicz[1]
[1]*Institute of Electrical Energy Conversion, University of Stuttgart, Germany, info@iew.uni-stuttgart.de*

Abstract

This paper deals with fundamental design criteria of stationary and dynamic wireless power transfer for electric vehicles and the development of a highly efficient system to supply trams without catenary. After describing the physical principle and mathematical relationships, requirements and characteristics of trams will be analyzed and used for a suitable system architecture. Then, parameters of windings, power electronics, and power compensation networks will be specified. Furthermore, the system's performance and transfer behaviour will be evaluated.

1 Introduction

Wireless charging of electric vehicles (EV), also known as Contactless Energy Transfer (CET) or Inductive Power Transmission, is becoming more and more popular since it provides a number of advantages compared to conductive charging. However, Wireless Power Transfer (WPT) is not limited to automobiles but also rolling stock is under consideration [1].

Due to the comparatively large air gap between the primary and the secondary coils this type of energy transfer suffers from a high magnetic leakage flux which might lead to a low efficiency and low power transfer capability. This can be reduced by using both an appropriate reactive power compensation network and a high frequency supply [2].

2 Fundamentals of Contactless Energy Transfer

In principle, energy can be transferred via any type of field. It is common to use the magnetic field changing over time as an energy carrier, while for some applications it is more useful to use either the electric field or electromagnetic waves. For short distance applications, where the distances to overcome are much shorter than the wavelength arising from the used frequency, energy transfer via the magnetic field is the most effective method, since it contains the highest energy.

2.1 Magnetic Coupling and Equivalent Circuits

The physical principle of CET can be shown by the consideration of conventional transformers. Two coils, the primary and secondary windings, are linked by the magnetic flux which is changing over time in the common core. The principal layout of a conventional transformer is illustrated in Fig.1 a). The flux created by the magnetic field can be divided into the main and the leakage flux. Fig.1 b) shows the corresponding magnetic equivalent circuit (MEC) which will be used to determine the physical parameters of the setup [3].

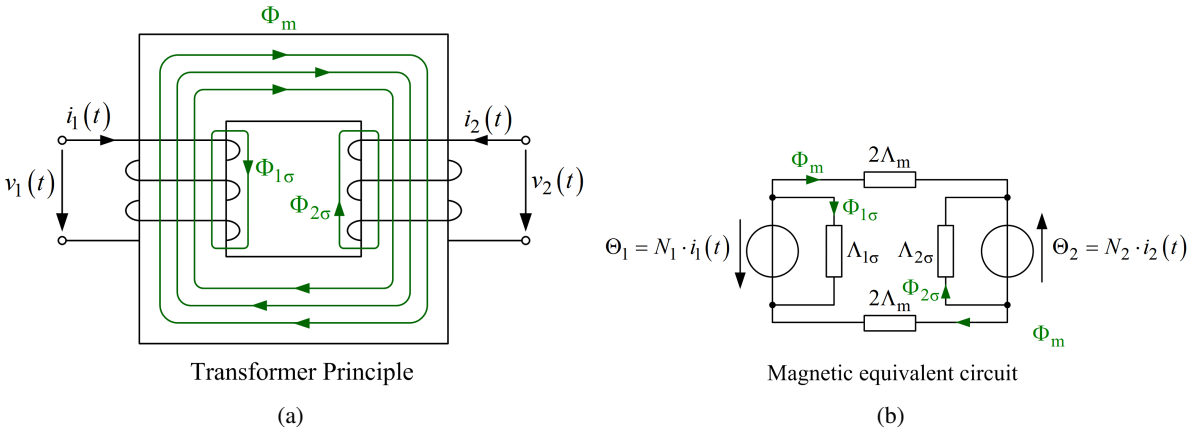

Figure 1: a) Principal layout of a transformer and b) corresponding magnetic equivalent circuit

The magnetic coupling coefficient k expresses a relationship between the magnetic leakage permeances and the magnetic main permeance and is an indicator for the coupling strength. k results from the system's geometry and can be gained from the magnetic equivalent circuit via the following equations:

$$k = \sqrt{k_{12} \cdot k_{21}} \tag{1}$$

$$= \sqrt{\frac{\Phi_m}{\Phi_1} \cdot \frac{\Phi_m}{\Phi_2}} \tag{2}$$

$$= \frac{1}{\sqrt{\left(\frac{\Lambda_{1\sigma}}{\Lambda_m} + 1\right) \cdot \left(\frac{\Lambda_{2\sigma}}{\Lambda_m} + 1\right)}} \tag{3}$$

where

k_{ij} is the coupling coefficient from coil i to coil j,

Φ_m is the main magnetic flux,

Φ_i is the total magnetic flux created by coil i

$\Lambda_{i\sigma}$ is the leakage permeance of coil i

Λ_m is the main permeance.

These geometric equations can be converted into expressions with inductances. With a relation for the inductances: $L = \Lambda \cdot N^2$, we obtain another common formulation for the coupling coefficient given in (4), where L_1 and L_2 stand for the inductances of primary respectively secondary coil:

$$k = \frac{M}{\sqrt{(L_{1m} + L_{1\sigma}) \cdot (L_{2m} + L_{2\sigma})}} = \frac{M}{\sqrt{L_1 \cdot L_2}} \tag{4}$$

Using the voltage equations of the primary and the secondary circuits leads to the electric equivalent circuit shown in Fig.2.
So far, all these considerations apply for both transformers and inductive power transfer systems. The difference between them is the relation between main flux Φ_m and the leakage fluxes $\Phi_{1\sigma}$ and $\Phi_{2\sigma}$. In transformers, $\Phi_m >> \Phi_{1\sigma}$ is valid, whereas in CET-systems due to the loosely coupled coils the leakage flux is much higher. The otherwise inevitable reduction in efficiency can be avoided by using capacitive compensation [4].

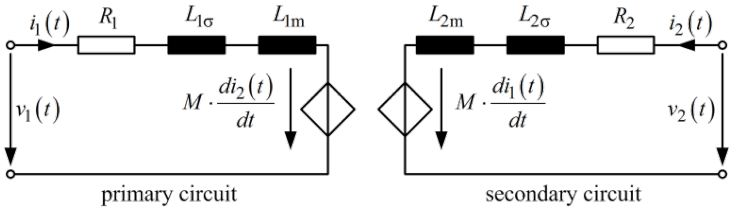

Figure 2: Electric equivalent circuit of the transformer setup

2.2 Reactive Power Compensation Networks

Because of the high leakage inductances, a coil system with a large air gap leads to a higher amount of reactive power than effective power that can be transferred over the air gap. Providing the required reactive power by power electronics would generate losses in them. A reasonable solution is to use capacitors as energy storages for the reactive power needed. Depending on the connection (series or parallel) and on the number of capacitors, this results in different resonance circuits with different system behaviour, respectively [5]. A series compensation on both, primary and secondary side, results in a constant-current-characteristic [6] and is shown as an example in Fig.3.

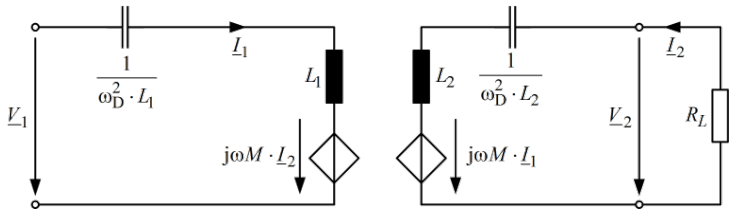

Figure 3: Simplified electric equivalent circuit for a series-series-compensated CET-system, which is one example for reactive power compensation

2.3 Power electronics

Starting from a DC-link with a given voltage, the power electronics to supply the winding system consist of a DC-link capacitor and the inverter circuit, converting direct current into an alternating, sinusodial current. This can most easily be realized by a full-brigde inverter made up of four transistors, as seen in Fig.4. Another possibility is to use an auto-resonant converter like the Royer-converter, that has the ability to always stay in resonance, without adjustment of component tolerances or aging effects. However, that means a change in design frequency, and therefore, a possible decrease in performance.

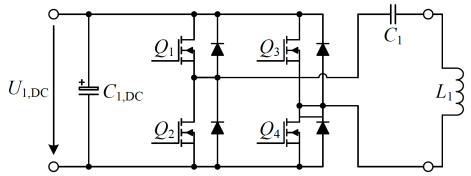

Figure 4: Primary side power electronics: DC-link voltage source, DC-link capacitor $C_{1,\mathrm{DC}}$, full-bridge inverter, compensating capacitor C_1 and primary winding L_1.

On the secondary side, a rectifier is needed to transform the alternating voltage obtained from the secondary winding into a DC-voltage that can be used to charge batteries or the like. In this example, a passive rectifier consisting of four diodes is being used (see Fig.5). To enable bidirectional power transfer it is also possible to replace the diodes with transistors for active rectification.
Performing a network analysis for the entire system yields an optimal load resistance $R_{L,\mathrm{opt}}$, that has to be connected to $U_{2,\mathrm{DC}}$:

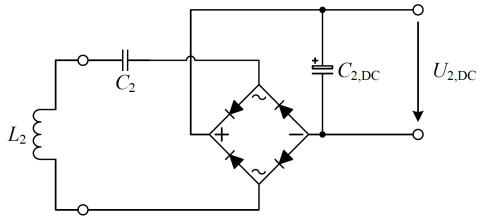

Figure 5: Power electronics on the secondary side: secondary winding L_2, a passive rectifier consisting of four diodes, a DC-link capacitor $C_{2,\mathrm{DC}}$ and the gained DC-voltage $U_{2,\mathrm{DC}}$.

$$R_{L,\mathrm{opt}} = \omega_0 L_2 \cdot \sqrt{2 - 2\sqrt{1-k^2}} \tag{5}$$

In CET-systems, the coupling factor k is smaller than 0.5, so that eq. (5) can be approximated by the following equation:

$$R_{L,\mathrm{opt}} \approx k\omega_0 L_2 \tag{6}$$

To design a system with a required rated power of about 1,200 kW, it is neccessary to evaluate currents and voltages on the secondary side. Given an ideal rectifier with smoothing capacitor, the relations between RMS and DC values is given by:

$$I_{2,\mathrm{DC}} = \frac{2\sqrt{2}}{\pi} \cdot I_{2,\mathrm{RMS}} \approx 0.9 \cdot I_{2,\mathrm{RMS}} \tag{7}$$

Results for the optimal load resistance, currents and voltages as well as the operating frequency are given in the next chapters.

3 System Design

3.1 Requirements for Catenary-free Light Rail

An inductive power supply system for trams has two main components: the primary windings located in the railroad and the secondary coil used as a pick-up located in the tram underfloor. To design a system, apart from electric requirements geometric parameters have to be considered as well.

World-wide, the majority of electric rail transport is fed by DC voltage. For smaller traction power commonly used in short-distance traffic, direct current voltage is more convenient due to safety reasons and lower inductive losses. Typical values for the power supply are 600 V and 750 V DC [7].

Next to electric requirements the main influence on the behaviour of an contactless energy transfer system is given by the geometric design of the primary and secondary windings. Therefore, the preexisting installation space presets the geometric boundary conditions for the system dimensioning. In this paper, we define the propagation axis of the trams as the y-axis, the cross-section of the tracks as the x-axis and, consequently, the height above the tracks as the z-axis.

Trams in Europe use the standard gauge of 1435 mm since also (heavy) rail transport lines are being used for transregional traffic. To avoid eddy currents in the rails, the wires for the primary coils should be placed inside this gap with an exemplaric width of $d = 1$ m between the conductors. Using slab tracks instead of ballasted tracks for installation increases both stability and durability of the CET-system. One possible coil arrangement can be seen in Fig.6, with a coil spread out along the y-axis, giving approximately two parallel conductors. Next to this type other topologies are possible, for example a meander type [8], which will not be further considered in this paper.

Most trams have a total length between 25 and 45 meters [9, 10]. While it is theoretically possible to equip the whole tram with just one or very few secondary coil windings, it is more convenient to have more and shorter secondaries. First, this gives the system more redundancy: If one coil system fails, it just means a decrease in performance and not a complete loss of function. Second, with matching primary sides, a more precise energy transfer is possible, since only the segments on which the tram is located have to be turned on. This is especially valid for wireless charging during stops at stations. Third, metallic elements interacting with the magnetic field like bogies and wheels will be protected

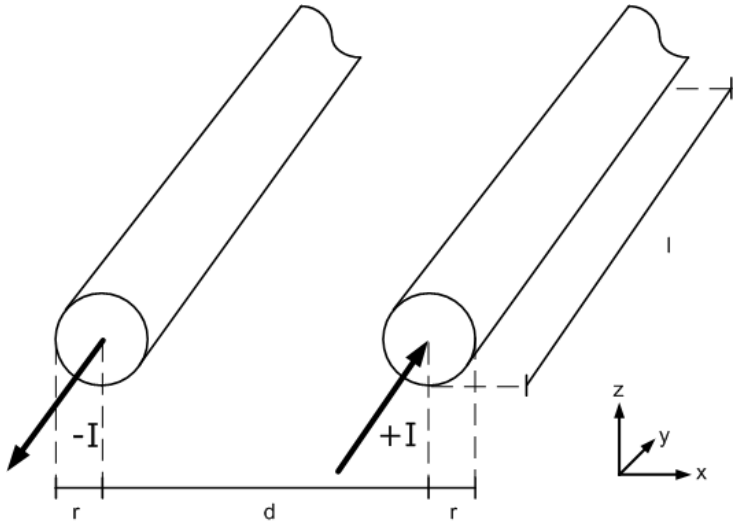

Figure 6: Arragement of primary windings with radius r and distance d placed between the rails. The tram moves in y-direction.

against unwanted heating. Considering these points leads to a higher overall efficiency. Therefore, a typical segment length for the secondary side is set to 3.6 m in this paper.

One of the challenges when designing a CET-system is to overcome the magnetic resistance in the air gap while remaining a high efficiency, which can be achieved by an appropriate reactive power compensation and the use of high operating frequencies (see section 2). Due to regulations in the General Railway Act there is a minimum clerance outline that has to be observed. In rolling stock applications the air gap ranges therefore between 15 cm and 30 cm, depending on which structures are being used for the installation. In the next chapter we calculate the coupling factor analytically for the regarded air gaps. Fortunately, once the system is designed, the variations in z-direction can be neglected, since the tram is being rail-guided; so that there is no severe variation of the coupling factor and hence no change in the other design parameters.

3.2 Basic concept

A principal outline how a segmentation on the primary side can be realized is shown in Fig.7. The supply section feeds the track, that consists of a circuit breaker, a rectifier and a disconnector to isolate the DC-link. Another disconnector is useful to deactivate the winding system, which is fed by inverters (see section 2.3).
The studied coil arrangement was already shown in Fig.6. Using Ampere's law and neglecting effects from contributions in y-direction emerging from the finite conductor length, the distribution for the magnetic flux density in the x-z-plane can be calculated analytically:

$$B_z(x,z,t) = \frac{\mu_0 \cdot i(t)}{2\pi} \cdot \left(\frac{x-a}{(x-a)^2 + z^2} - \frac{x-b}{(x-b)^2 + z^2} \right), \tag{8}$$

where μ_0 denotes the magnetic constant $\mu_0 = 4\pi \cdot 10^{-7}$ H/m; i(t) denotes the alternating current (labeled "$\pm$I" in Fig.6); a is the position of conductor 1 and b the position of conductor 2. In Fig.8, the magnetic flux density in z-direction is plotted against the position x for several air gap distances z. The conductors are positioned at a = -0.5 m and b = 0.5 m. Note that the underlying current was set to 2000 ampere turns and only the maximal value, i.e. $i(t) = \hat{i}$, was plotted here.
With the magnetic flux density B_z given, the magnetic flux Φ can be calculated by:

$$\Phi = \iint_A \vec{B} \cdot \, d\vec{A} = \iint_A \vec{B} \cdot \vec{n} \cdot \, dA \tag{9}$$

The scalar product in eq. (9) is maximal, when the normal vector $\vec{n}$ is parallel to the flux density $\vec{B}$, i. e., when the secondary conductor loop is perpendicular to the field lines. This assumption is valid for tram applications, since primary and secondary windings are concentric and not tilted to each other. For

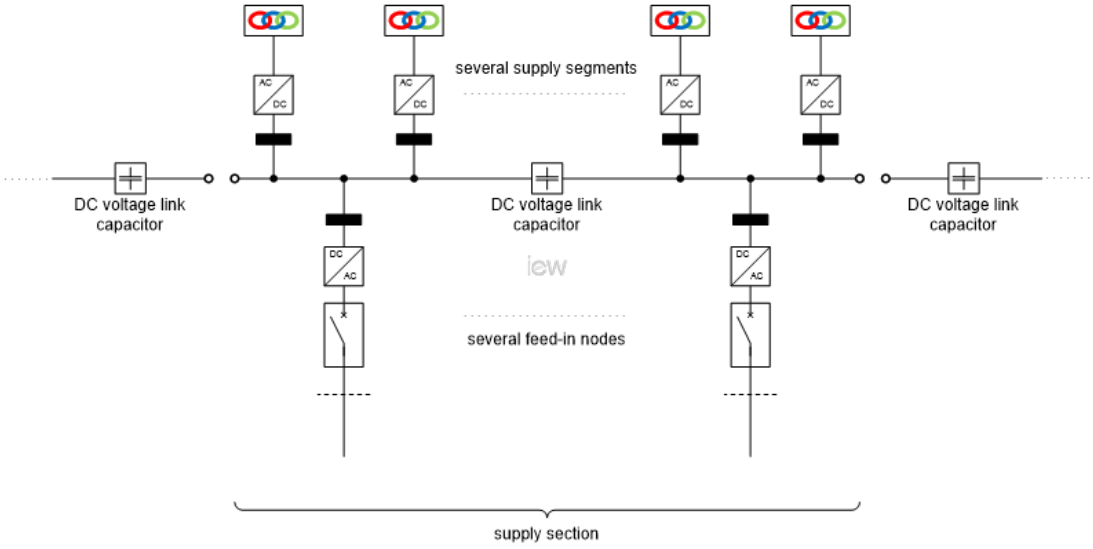

Figure 7: Exemplary system outline of an primary side with several feed-in nodes

a secondary side of 1 m x 1 m, the flux Φ can be determined from the calculated flux density B_z and is plotted in Fig.9.
As indicated in section 2.1, there are different methods to obtain the coupling factor k. For an existing coupled coil arragement, k can be measured indirectly by measuring the inductances L_1, L_2, M and using eq. (4). Given the geometric dimensioning and the resulting magnetic fluxes, it is most convenient to use eq. (2), expressed as:

$$k = \sqrt{k_1 \cdot k_2} = \sqrt{\frac{\Phi_{21}}{\Phi_1} \cdot \frac{\Phi_{12}}{\Phi_2}} \tag{10}$$

Here, Φ_i is the total flux created by coil i and Φ_{ij} is the flux through coil i produced by coil j. With the magnetic flux, it is also possible to calculate the inductance per unit length (under the assumption, that the radius r is much smaller than the distance d):

$$L' = \frac{L}{l} = \frac{N \cdot \Phi}{I \cdot l} = \frac{\mu_0}{\pi} \cdot \left(\frac{1}{4} + \ln\left(\frac{d}{r} \right) \right) \tag{11}$$

With those considerations, the coupling factor k for conductors of radius r = 8 mm (corresponds to a typical wire cross section of about 200 mm^2) and distance d = 1 m can be plotted against the vertical position (height) of the secondary coil, as seen in Fig.10. For the required air gaps of about 0.15 m to 0.30 m, the coupling factor ranges between 0.38 and 0.25, which is in good accordance to typical values for CET-systems.

3.3 Evaluation of performance

With the results from the last section, technical design details of the primary and secondary side for an exemplary CET-system with a rated power of 1,200 kW can be presented.
The distance d between the conductors should be kept to 1 m for both coils, since it allows maximum coverage and hence optimal coupling. The secondary side was already chosen to 3.6 m; the primary side should be noticable shorter for the reasons already mentioned in section 3.1. Here, we chose a length of 1.8 m for the primary side to simplify the calculations. Given the possibility to equip the tram with more than one secondary side, the rated power per segment is smaller than the total rated power. For an exemplary study of a total rated power of 1,200 kW and three secondary side pick-up segments, the rated power per segment is defined in this paper to 500 kW to have a safety margin. That yields an requested current of $I_{2,\mathrm{RMS}} \approx 740$ A and a voltage of $U_{2,\mathrm{RMS}} \approx 675$ V. With a wire cross section of 200 mm^2, the inductance per meter is about $L_2' \approx 2$ µH. It is useful to enhance the inductance by increasing the number of turns, since it means linear rise in losses, but quadratic increase of coupling. Still, weight issues and installation space requirements have to be met. Therefore, we decided to design the secondary side with two turns: N_2 = 2, which leads to a total inductance of $L_2 \approx 30$ µH.

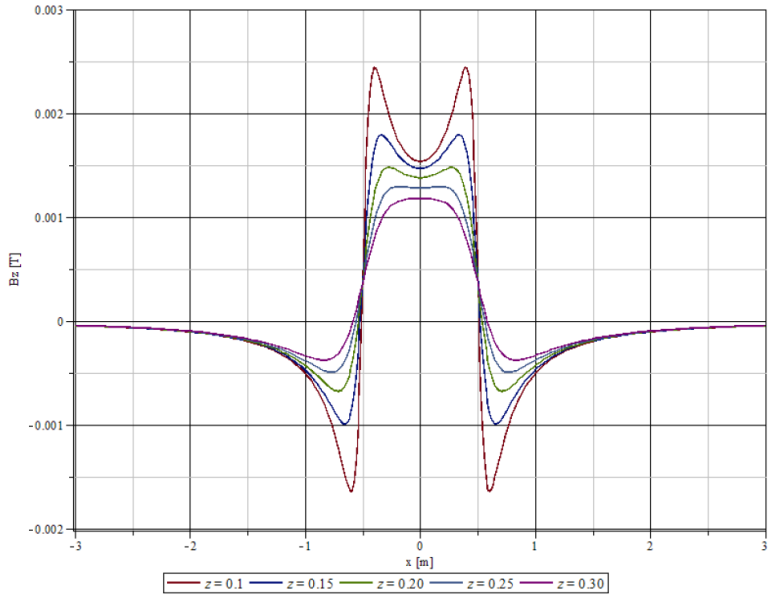

Figure 8: Analytical result of the magnetic flux density in z-direction, B_z, depending on the position x for different air gaps z at an underlying current of 2000 ampere turns

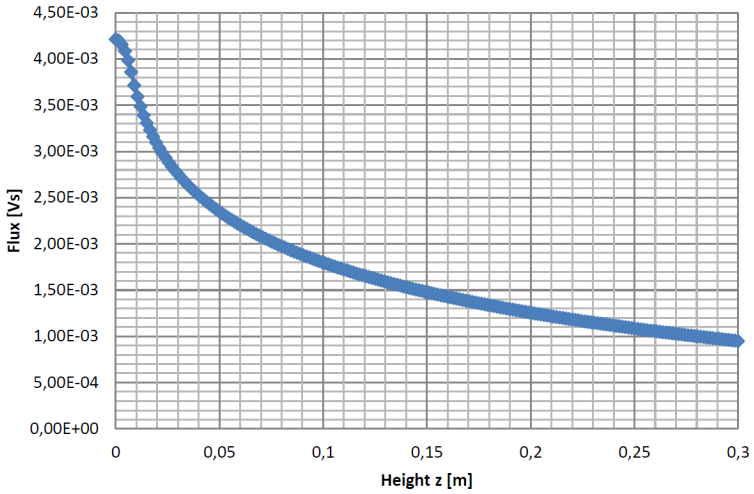

Figure 9: Analytical result of the flux Φ through a secondary coil with an area of 1 m^2

Compared to the results obtained in section 3.2, the primary side is shorter and therefore it is assumed that the coupling factor k decreases to values between 0.15 and 0.25. For an exemplary coupling factor of 0.15, it is neccessary to increase the operating frequency to maintain the desired voltage on the secondary side (by maintaining the optimal load resistance, see eq. (6)). This results in a design frequency of 32.3 kHz, which also defines the capacitance for C_2:

$$C_2 = \frac{1}{\omega_D^2 \cdot L_2} \tag{12}$$

To evaluate the ohmic losses, a slightly reduced conductivity for the litz wires compared to mere copper was set to $\sigma = 50 \cdot 10^6$ S/m. For the configuration evaluated in this paper, this results in a resistance of 1.84 mΩ for the secondary coil and 1.12 mΩ for the primary coil. The power losses due to ohmic resistance amount to approximately 0.9 kW on the primary side and 3.1 kW on the secondary side. Compared

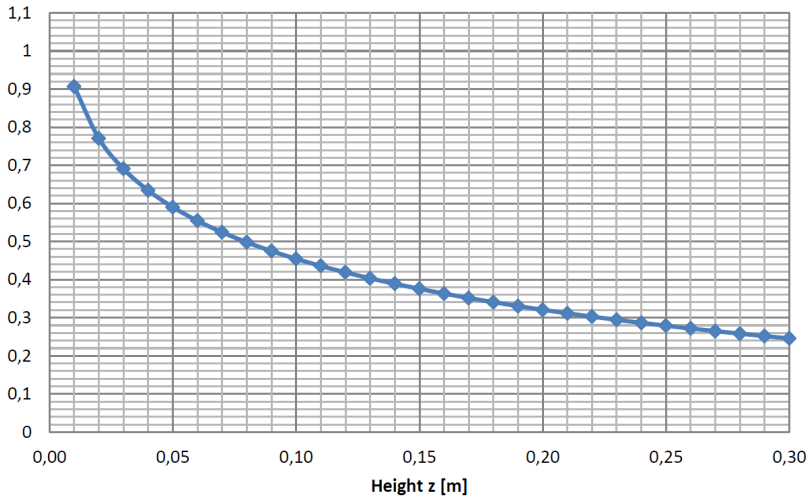

Figure 10: Analytical result of the coupling factor k depending on the height of the secondary winding

to the rated power, these relative losses correspond to 0.26 %.

4 Conclusion

In this paper, a design possibility for a CET-system in tram applications was investigated. Boundary conditions were given by geometric considerations as well as a desired rated total power of 1,200 kW. The CET-system itself consisted of a line conductor type primary and secondary side, series compensation on both sides as well as full-bridges with transistors for the inverter and with diodes for the rectifier, respectively. Considering only ohmic losses, the CET-system would have an efficiency of approximately 99.7 %. Nevertheless, losses resulting from switching in the power electronics, eddy currents and hysteresis cannot be neglected for a real system and may require an additional cooling system.

References

[1] J. Heinrich et al. *Contribution to the development of Inductive Power Supply for Heavy Rail Vehicles.*, ETG-Fachbericht-Internationaler ETG-Kongress 2013 - Energieversorgung auf dem Weg nach 2050. VDE VERLAG GmbH, 2013.

[2] M. Zimmer, J. Heinrich and N. Parspour, *Design of a 3 kW primary power supply unit for inductive charging systems optimized for the compatibility to receiving units with 20 kW rated power*, 4th International Electric Drives Production Conference (EDPC), Nuremberg, 2014, 1-5.

[3] P. C. Sen, *Principles of Electric Machines and Power Electronics,* ISBN 0-471-02295-0, John Wiley & Sons, 1996.

[4] C. Chen, T. Chu, C. Lin, Z. Jou *A Study of Loosely Coupled Coils for Wireless Power Transfer*, IEEE Transactions on Circuits and Systems II: Express Briefs (Volume: 57, Issue: 7, July 2010).

[5] D. Maier, J. Heinrich, M. Zimmer, M. Maier, N. Parspour *Contribution to the System Design of Contactless Energy Transfer Systems*, International Power Electronics and Motion Control Conference (PEMC), 2016.

[6] K. Aditya, S. Williamson *Simplified Mathematical Modelling of Phase-Shift Controlled Series-Series Compensated Inductive Power Transfer System*, 25th International Symposium on Industrial Electronics (ISIE), 2016.

[7] H. Biesenack, G. George, u.a. *Energieversorgung elektrischer Bahnen,* ISBN 978-3519062493, Vieweg+Teubner, 2006.

[8] F. Turki, V. Staudt, A. Steimel *Dynamic wireless EV charging fed from railway grid: Magnetic topology comparison*, International Conference on Electrical Systems for Aircraft, Railway, Ship Propulsion and Road Vehicles (ESARS), 2015.

[9] ALSTOM product sheet *CITADIS (R) X05/EN/09.2016*, online: www.alstom.com, June 2017.

[10] Siemens AG product sheet *Strassenbahn Avenio (R) Munich*, online: www.siemens.com/mobility, June 2017.

Authors

Nejila Parspour is Professor of Electrical Energy Conversion at the University of Stuttgart and head of the Institute of Electrical Energy Conversion. She received her Master in electrical engineering in 1991 and her PhD (summa cum laude) in 1995, both from Technical University of Berlin. Before joining the University of Stuttgart she collected 5 years of industrial experience at Philips and 6 years of scientific experience at the University of Bremen. Her research and teaching activities are in the field of electrical machines and drives with a focus on machine design and in the field of contactless energy transfer with a focus on inductive charging systems.

Philipp Seitz is a research associate at the Institute of Electrical Energy Conversion, University of Stuttgart. He received his diploma in electrical engineering from the University of Stuttgart in 2011 and is currently doing a PhD. His research activities cover contactless energy transfer with a focus on inductive power transmission for railway vehicles.

Anna Lusiewicz is a research associate at the Institute of Electrical Energy Conversion at the University of Stuttgart. She received her diploma in theoretical physics from the University of Muenster in 2013 and is currently a PhD student in electrical engineering. Her research interest is dynamic contactless energy transfer on moving objects with a focus on mathematical modelling.